Screened Coulomb interaction in insulators with strong disorder

V. A. Stephanovich ⬤, W. Olchawa, and E. V. Kirichenko ⬤

Institute of Physics, University of Opole, Oleska 48, 45-052, Opole, Poland

We study the effect of disorder on the excitons in a semiconductor with screened Coulomb interaction. Examples are polymeric semiconductors and/or van der Waals structures. In the screened hydrogenic problem, we consider the disorder phenomenologically using the so-called fractional Scrödinger equation. Our main finding is that joint action of screening and disorder either destroys the exciton (strong screening) or enhances the bounding of electron and hole in an exciton, leading to its collapse in the extreme case. Latter effects may also be related to the quantum manifestations of chaotic exciton behavior in the above semiconductor structures. Hence, they should be considered in device applications, where the interplay between dielectric screening and disorder is important. Our theoretical results permit one to predict the various excitonic properties in semiconductor samples with different degrees of disorder and Coulomb interaction screenings.

I. INTRODUCTION

Disordered and amorphous semiconductors have impressive functional properties and are therefore useful for technological applications, see [1] and references therein. Despite remarkable advances in the understanding of exciton creation and dissociation in the above highly disordered semiconductors, important questions still remain [2–6]. For example, as the dielectric screening is particularly strong in semiconductors and can be well described by the band theory, inherent in perfectly ordered substances, its influence on exciton properties in strongly disordered substances remains unclear. That being said, the joint action of (strong) disorder and dielectric screening on the exciton properties is not well understood to date. One of the basic physical mechanisms here is so-called compositional disorder, i.e., the exciton scattering by fluctuations of the crystal composition. Such kind of disorder is always present in the semiconductor structures, and it is especially important in magnetooptical and photovoltaic applications [7]. The magnetooptical effects, being most prominent in diluted magnetic semiconductors like $Cd_{1-x}Mn_xTe$, are highly sensitive to the above composition fluctuations [7]. Many additional types of disorder occurs in semiconductor structures, used for photovoltaic applications [2,6,8,9]. To name a few, these are chemical impurities, dislocations, conformational and structural disorders in polymeric substances, etc. [10]. These impurities may not only adversely influence the functionality of an electronic device but can also play a useful role. Namely, the varying degree of disorder (e.g., by doping) gives one more possibility to control the physical properties of the substance, which can be useful for the proper functioning of a corresponding device. This is the case for $Cd_{1-x}Mn_xTe$ [7], where the amplitude of randomizing potential can be easily controlled by x variation. It is well known, that the noninteracting, individual point defects (the usual case of weak disorder) can be traps for excitons. The properties of such systems are already well understood [11].

On the other hand, when we have a strong disorder, leading to substance amorphization, we know neither the details of the exciton creation process nor its properties. As the latter effects are significant for proper functioning of photovoltaic cells, nanolasers, and light-emitting diodes [12,13], the theoretical understanding of strong disorder effects is highly desirable.

It is common knowledge that the weak disorder can be well described by the Gaussian distributions. This is because the width of the latter distribution is always small, corresponding to an almost ordered situation. If the concentration of defects and/or impurities is large, the randomness becomes high so that the width of the corresponding distribution increases. In this case, the Gaussian approximation is often insufficient so that more general distributions should be utilized [14]. Such non-Gaussian distributions emerge naturally in many physical systems, ranging from charge transport in amorphous solids and optical lattices to the excitons in semiconductors [15–20]. Note that in the above systems, the unjustified substitution of actual non-Gaussian distributions by Gaussian ones leads often to cataclysmic results [15,20,21], especially in more than one spatial dimension. The convenient phenomenological tool to model non-Gaussian distributions is so-called fractional derivatives, see [22,23] and references therein. These derivatives, in particular, generate so-called Lévy stable probability distributions [24–26], which are used widely to describe non-Gaussian properties of many physical, chemical, biological, and financial entities [26–30]. Furthermore, it's worth mentioning that using fractional Laplacians in random walks won't produce Lévy stable distributions. Rather, the corresponding propagators only share the asymptotics with latter distributions.

One more application of non-Gaussian processes is so-called fractional quantum mechanics [31], dealing with the substitution of the ordinary Laplacian with the fractional one in the corresponding stationary Schrödinger equation. In the

n-dimensional case, the definition of the fractional Laplacian reads

$$|\Delta|^{\mu/2} f(\mathbf{x}) = -A_{n,\mu} \int \frac{f(\mathbf{u}) - f(\mathbf{x})}{|\mathbf{u} - \mathbf{x}|^{\mu+n}} d^n u, \qquad (1)$$

$$A_{n,\mu} = \frac{2^\mu \Gamma\left(\frac{\mu+n}{2}\right)}{\pi^{n/2} |\Gamma(-\mu/2)|}, \qquad (2)$$

where $\mathbf{x}$ is an n dimensional vector and $0 < \mu < 2$ is so-called Lévy index. In our case, the Lévy index will play the role of a descriptor of a degree of disorder, see below. Also, here $\Gamma(x)$ is Γ-function [32]. The operator (1) is spatially nonlocal with a slowly decaying power-law kernel (dictated by Lévy index as well as spatial dimensionality) typical for memory effects in complex disordered systems.

In the present paper, we focus on the influence of Coulomb interaction screening on the excitons properties in highly disordered (see above) insulators. To accomplish this task, we solve a hydrogenic problem which is defined by a Schrödinger equation with screened Coulomb potential and fractional Laplacian. Latter substitution mimics the disorder phenomenologically and constitutes the simplest possible exciton description which captures the main physics of the problem. Our main point here is that charge carriers (electrons or holes) in highly disordered substances are located not in a periodic crystalline potential, but rather in some distorted (by the disorder) one. This implies that in this case, the famous Bloch's theorem is no longer valid. Therefore, electronic states are not expected to be periodic Bloch functions. This means, in turn, that in amorphous substances, the band theory of solids, based on the perfect translational symmetry, is inapplicable, see, e.g., [11]. In other words, strong disorder destroys any symmetry of the initial (before, say, doping) crystalline structure. Hence, amorphous semiconductors of any original symmetry behave similarly to each other, resembling, say, isotropic ceramics. That is why, for our purposes, it is sufficient to consider the above simplest possible effective mass model of an exciton.

II. GENERAL FORMALISM

To model the problem of a "screened exciton" in a disordered semiconductor (dielectric), here we consider a fractional (mimicking disorder) hydrogenic problem in the screened Coulomb potential. It is wellknown (see, e.g., [33]), that the ordinary quantum mechanical hydrogenic problem is related to the excitons (bound states between electrons and holes, see Ref. [33,34] for details) description in semiconductors.

With definition (1) at hand, the fractional Schrödinger equation for the above screened hydrogenic problem reads

$$-|\Delta|^{\mu/2}\Psi_{nlm\mu}(\mathbf{r}) - \frac{2e^{-\frac{r}{r_0}}}{r}\Psi_{nlm\mu}(\mathbf{r}) = E_{nlm\mu}\Psi_{nlm\mu}(\mathbf{r}). \quad (3)$$

Here n, $l \leqslant n$, and m stand for the principal, orbital, and magnetic (z projection of orbital momentum) quantum numbers and $\mathbf{r}$ is a radiusvector. Note that quantum numbers n, l, and m are different for different μ's. We will see below that for $\mu < 2$ the orbital degeneracy is lifted, which is the reason why the eigenenergy E acquires the dependence on the orbital quantum number. At the same time, as the time-reversal

symmetry in our case (without external magnetic field) is conserved, we still have degeneracy with respect to sign and value of the quantum number m. We explicitly include the index m in the wave functions in Eq. (3) just to demonstrate that they differ for different $-l < m < l$, even though the energy E is the same for all m, which correspond to the given l.

Here we use modified (for the fractional case $\mu < 2$) Rydberg units [31], i.e., we measure the energy E and coordinates $\mathbf{r}$ in the units

$$E_{0\mu} = \left(\frac{\beta}{2\hbar}\right)^{\frac{\mu}{\mu-1}} D_\mu^{-\frac{1}{\mu-1}}, \; r_{0\mu} = \left(\frac{2\hbar^\mu D_\mu}{\beta}\right)^{\frac{1}{\mu-1}}, \quad (4)$$

respectively. Here β is a coefficient in front of (dimensional) screened Coulomb potential:

$$U(r) = -\frac{\beta}{r} e^{-\frac{r}{r_0}}, \quad (5)$$

D_μ is a mass term [31]. At $\mu = 2$ $D_2 \equiv \frac{1}{2m}$ (m is a real physical mass), and we have the standard Rydberg units from (4). Note that at $\mu = 1$ both quantities $E_{0,\mu=1}$ and $r_{0,\mu=1}$ in (4) are divergent. Below we will see that this reflects the actual situation with our problem, i.e., that discrete spectrum exists for $\mu > 1$ only [31,35].

It is well-known that integral (1) exists only in the sense of its Cauchy principal value [22,23]. This already complicates the solutions of spectral problems like (3) for pseudodifferential operators [23]. Our analysis shows that it is much more profitable to pass to the momentum space (i.e., perform Fourier transformation) as the operator (1) becomes simply $-|\mathbf{k}|^\mu$. Although in this case the potential term (5) converts to an integral, it is much easier to deal with than the initial one (1). Moreover, in passing to momentum space, the angular integration can be done exactly without expansion over spherical harmonics (which is customary in quantum hydrogenic problems for $\mu = 2$ [36,37]) giving close form representation of the Eq. (3) in momentum space. Latter representation permits to solve the corresponding fractional Schrödinger equation both numerically and variationally. To find the eigenfunctions in the coordinate space, we perform inverse Fourier transformation.

To transit to momentum space, we apply a Fourier transformation to both parts of Eq. (3). This generates the following equation in momentum representation:

$$\left(k^\mu + k_0^\mu\right)\Psi(\mathbf{k}) - \frac{1}{\pi^2} \int d^3k' \frac{\Psi(\mathbf{k}')}{|\mathbf{k} - \mathbf{k}'|^2 + 1/r_0^2} = 0, \quad (6)$$

where the indices $nlm\mu$ are suppressed for clarity. Here, similar to the case of an ordinary hydrogen atom, we denote

$$E = -k_0^\mu. \quad (7)$$

It is easy to see that at $\mu = 2$ and $r_0 \to \infty$, the Eq. (6) yields well-known $\mathbf{k}$-space representation of ordinary unscreened hydrogen atom [36].

As the potential (5) is central, the wave functions are invariant under the rotation about the origin [38]. This implies the usual separation of radial and angular variables. Latter fact permits to represent the solution in the form

$$\Psi_{nlm\mu}(\mathbf{k}) = \psi_{nl\mu}(k) Y_{lm}(\theta, \varphi), \quad (8)$$

where $Y_{lm}(\theta, \varphi)$ are spherical functions [32,39]. Their normalization conditions reads [39]

$$\int_0^{2\pi} d\varphi \int_0^{\pi} Y_{lm}^*(\theta, \varphi) Y_{lm}(\theta, \varphi) \sin\theta d\theta = 1. \qquad (9)$$

The normalization condition (9) permits to reduce that for 3D wave functions (8)

$$\int \psi^*(\mathbf{k})\psi(\mathbf{k})d^3k = 1 \qquad (10)$$

to the effective 1D form

$$\int_0^{\infty} \psi^2(k)k^2 dk = 1, \qquad (11)$$

where we suppress lower indices for a moment.

Integration over angular variables θ' and φ' in (6) yields

$$\left(k^{\mu} + k_0^{\mu}\right)\psi_{nl\mu}(k) - \frac{2}{\pi k}\int_0^{\infty} Q_l(z)\psi_{nl\mu}(k')k' dk' = 0,$$

$$z = \frac{k^2 + k'^2 + 1/r_0^2}{2kk'}, \qquad (12)$$

where we restore index μ, and $Q_l(z)$ are Legendre polynomials of the second kind [32].

As our problem is symmetric with respect to time inversion $t \rightarrow -t$ (see [36,39]), the wave functions in Eq. (12) do not depend on quantum number m. Former symmetry exists at zero magnetic fields and makes the radial wave functions $\psi_{nl\mu}(k)$ real [39]. The Schrödinger equation (12) for each l defines the spectrum of fractional screened hydrogenic problem for that particular l and the principal quantum number $n > l$. The representation (12) reduces the 3D spectral problem (6) for each specific l to an effective 1D integral equation.

III. VARIATIONAL SOLUTION

It is common knowledge that the variational principle of quantum mechanics [39] permits to find the approximate analytical expressions for the wave functions and eigenenergies of corresponding Schrödinger equations. This is especially true for the states of discrete spectrum, which are spatially localized. In our case, the above variational approach permits to get the approximate (which will be checked below by direct numerical simulations) spectrum of the fractional screened hydrogen atom for all admissible μ. To accomplish this, we rewrite Eq. (12) in the form

$$k^{\mu}\psi_{nl\mu}(k) - \frac{2}{\pi k}\int_0^{\infty} Q_l(z)\psi_{nl\mu}(k')k' dk' = E\psi_{nl\mu}(k), \quad (13)$$

where E is defined in (7). Multiplying both parts of (13) by $\psi_{nl\mu}(k)$ (no need for complex conjugation as radial functions are real) and integrating over $k^2 dk$, we obtain the following variational functional (here k_v is the variational parameter):

$$W_{\text{var}}(k_v) = W_{\text{kin}}(k_v) - W_1(k_v), \; W_{\text{kin}}(k_v)$$
$$= \int_0^{\infty} k^{\mu+2}\psi_{nl\mu}(k, k_v)dk, \; W_1(k_v)$$
$$= \frac{2}{\pi}\int_0^{\infty} k' dk' \int_0^{\infty} k dk \, Q_l(z)\psi_{nl\mu}$$
$$\times (k', k_v)\psi_{nl\mu}(k, k_v), \qquad (14)$$

where z is defined in (12). Now, to obtain the variational solution of our problem, we should substitute a properly orthonormalized function $\psi_{nl\mu}$ into $W_{\text{var}}(k_v)$ (14) and minimize the obtained function over $k_v \equiv k_{vnl}$, which depends on quantum numbers n and l. To do so, we need to construct the orthonormal set of trial wave functions. For that, we use the corresponding basis for the initial, unscreened problem (see, e.g., [36,40]) and modify it to our fractional case $\mu < 2$.

The radial functions for $\mu = 2$ in momentum space can be derived by the Fourier transformation of corresponding functions in coordinate space, see, e.g., [36]. Note that for $\mu < 2$, the famous orbital degeneracy (due to Runge-Lenz vector conservation [39]) of unscreened hydrogen atom eigenstates is lifted so that excited state energies begin to depend on orbital index l. The consequence of Runge-Lenz vector conservation at $\mu = 2$ is the fact that the above set of radial functions is n^2 fold degenerate [36,39]. The above suggests to choose the ground state function in the following normalized form

$$\psi_{10\mu}(k) = \frac{A_{10\mu} \, k_{v10}^{\mu+\frac{1}{2}}}{\left(k_{v10}^2 + k^2\right)^{\frac{\mu+2}{2}}}, \qquad (15)$$

where k_{v10} is a variational parameter and

$$A_{10\mu}^2 = \frac{4\Gamma(\mu + 2)}{\sqrt{\pi}\,\Gamma\left(\mu + \frac{1}{2}\right)}. \qquad (16)$$

We have four distinct functions $\psi_{20\mu}(k)$, $\psi_{21\mu}(k)\cos\theta$, $\psi_{21\mu}(k)\sin\theta e^{\pm i\varphi}$ for the first excited state ($n = 2$, $l = 0, 1$). This is because at $\mu = 2$ this state is fourfold degenerate. We will observe below that the energies for $\psi_{20\mu}(k)$ and $\psi_{21\mu}(k)$ differ, indicating that the introduction of the fractional Laplacian removes the angular degeneracy of the initial problem at $\mu = 2$. The functions $\psi_{20\mu}(k)$ and $\psi_{21\mu}(k)$ can be chosen in the following form

$$\psi_{20\mu}(k) = \frac{A_{20\mu} \, k_{v20}^{\mu+\frac{1}{2}}\left(k_{v20}^2 + Ck^2\right)}{\left(k_{v20}^2 + k^2\right)^{\frac{\mu+4}{2}}}, \qquad (17)$$

$$\psi_{21\mu}(k) = \frac{A_{21\mu} \, k \, k_{v21}^{\mu+\frac{3}{2}}}{\left(k_{v21}^2 + k^2\right)^{\frac{\mu+4}{2}}}, \qquad (18)$$

where

$$A_{20\mu}^2 = \frac{16\Gamma(\mu + 4)}{\sqrt{\pi}\,g(C, \mu)\Gamma\left(\mu + \frac{1}{2}\right)}, \qquad (19)$$

$$g(C, \mu) = 15C^2 + 6C(2\mu + 1) + 4\mu(\mu + 2) + 3,$$

$$A_{21\mu}^2 = \frac{8\Gamma(\mu + 4)}{3\sqrt{\pi}\,\Gamma\left(\mu + \frac{3}{2}\right)}. \qquad (20)$$

The value of the coefficient C in Eq. (17) is selected based on the orthogonality requirement $\langle \psi_{10\mu}(k)\psi_{20\mu}(k)\rangle = 0$, where $\langle...\rangle$ denotes the integral of the function over a specified range. It should be noted that functions with different values of l are already orthogonal due to the relationship described by Eq. (9) for spherical functions. This indicates that we only need to perform orthogonalization on functions with different values of n.

The construction shown here demonstrates our orthogonalization algorithm. Specifically, based on functions for $\mu = 2$

[40], we choose the functions for $\mu < 2$ (and given n and l) in the form of a quotient of two polynomials. The polynomial in the numerator has unknown coefficients, which are determined from the corresponding orthogonality conditions. Such a procedure can be readily continued for arbitrary n, although the expressions for trial functions become progressively more cumbersome. The procedure of minimization of the functional (14) shows that the solution to our variational problem exists at $\mu > 1$ only [31,35]. As we shall see below, our numerical solution of the integral equations (12) confirms this conclusion.

IV. NUMERICAL TREATMENT

Our next step is to solve Eq. (12) numerically. Performing substitutions $k/k_0 = x, k'/k_0 = y$ in it, we arrive at the following form of the Schrödinger equation, which is suitable for the numerical solution

$$\lambda \rho_{nl\mu}(x) = \int_0^\infty K_{l\mu}(x, y)\rho_{nl\mu}(y)dy,$$

$$\rho_{nl\mu}(x) = x\psi_{nl\mu}(x)\sqrt{x^\mu + 1}, \ \lambda = k_0^{\mu-1},$$

$$K_{l\mu}(x, y) = K_{l\mu}(y, x) = \frac{2}{\pi} \frac{Q_l\left(\frac{\xi^2(x^2+y^2)+1}{2\xi^2xy}\right)}{\sqrt{(x^\mu + 1)(y^\mu + 1)}},$$

$$\xi = k_0 r_0. \tag{21}$$

Expression (21) is a linear Fredholm integral equation [41], which can be easily discretized with the subsequent solution of the spectral problem for the obtained matrix. The eigenenergy of our problem E is related to the eigenvalues κ of the above matrix by the expression $E = -\lambda^{\frac{\mu}{\mu-1}}$. To obtain a satisfactory accuracy of the numerical solution of the eigenproblem (21), we should typically diagonalize a $10\,000 \times 10\,000$ matrix, which makes the task quite computer intensive.

We further derive the variational energies for the states $\psi_{nl\mu}$ as functions of Lévy index μ using (14) and compare them to numerical ones, obtained from (21). Note that the forms of variational wave functions are dictated by expressions (15) (ground state), (17), and (18) (first excited state) for parameters $k_{vnl\,\min}(\mu)$ as for $\mu > 1$, the energy extremum corresponds to a minimum. It is instructive to consider the well-known case of an "ordinary" hydrogen atom with an unscreened Coulomb interaction, corresponding to $\mu = 2$. In this case the solution of the problem is well studied (see [39] for coordinate space and [36] for momentum space) and its energy spectrum in our Rydberg units reads $E = -1/n^2$, $n = 1, 2, 3, \dots$. It is well-known that the ground state energy of a hydrogenic problem is proportional to exciton binding energy. This energy is reported in Fig. 1. Panel (a) displays the comparison of numerical (symbols) and variational (solid lines) dependencies of the ground state energy upon Lévy index μ at several fixed values of dimensionless screening radius ξ, shown as figures near curves. We intentionally put the numerical curve in the form of (not very much) symbols to better see the differences between variational and numerical dependencies. Namely, while for the unscreened case $\xi \to \infty$ the numerical and variational curves are almost (with the error
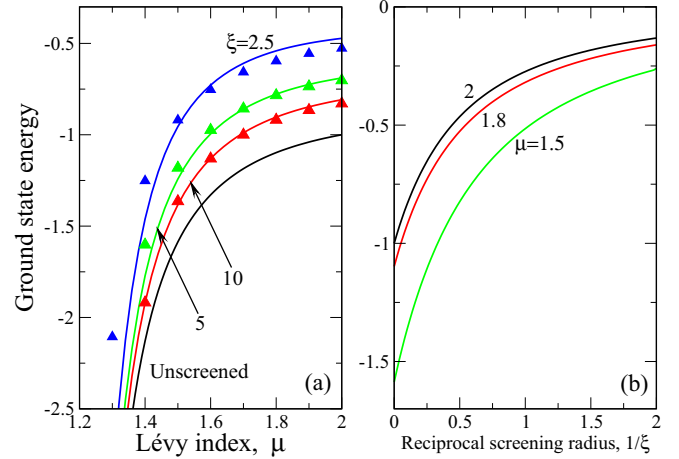

FIG. 1. (a) Reports the comparison of numerical (symbols) and variational (solid lines) ground state energies for different ξ (figures near curves) as functions of the Lévy index μ. For better visualization of the difference between numerical and variational curves, we present the former as symbols for several selected points. For the unscreened case ($\xi \to \infty$, black curve), the variational and numerical curves are identical in the scale of the plot. (b) Displays the numerical dependencies of ground state energy on reciprocal dimensionless screening radius $1/\xi$ for different μ (figures near curves).

less than 0.1%, which is invisible in the scale of the plot) the same; for $\xi = 2.5$ the coincidence is not that good with the average error around 10% at $\mu \sim 2$. This error increases even more as μ approaches one, i.e., the exciton existence boundary. The error grows also at $\xi < 2.5$. Our estimations show that maximal error can reach even 50%. At the same time, at $\xi > 2.5$, the accuracy of the variational approximation is around 1% and grows only at $\mu \lesssim 1.4$. The point here is that our trial functions (15)–(18) have been constructed for the wave function asymptotics (obtained from the integral Eq. (12), see [35] for details), which does not include the screening radius ξ. Another fact is that our trial functions contain only one variational parameter k_v [of course with other indices, distinguishing between corresponding states, see (15)–(18)], which comprises the simplest possible case. The consideration of more exact asymptotics, as well as adding more variational parameters, would improve the accuracy of the variational method but at the same time will make the calculations prohibitively complex. The latter can be seen from the expressions (19) and (20), where (already quite cumbersome) the parameters of trial functions (15)–(18) are listed. Note also that while for $\mu \gtrsim 1.5$, the variational energy lies higher than (say, exact) numerical, at $\mu \lesssim 1.5$ the situation is opposite. The former fact reflects the well-known situation with the variational method in quantum mechanics (see, e.g., [39]), where the exact energy (corresponding to numerical in our case) is the lowest value of the variational one. Moreover, it is achieved at an infinite number of variational parameters. In other words, the variational energy is always higher than the exact one [36,39]. We see from Fig. 1(a) that the variational energy is *lower* than "exact" (i.e., numerical) one, which shows that at this range of Lévy indices, the variational
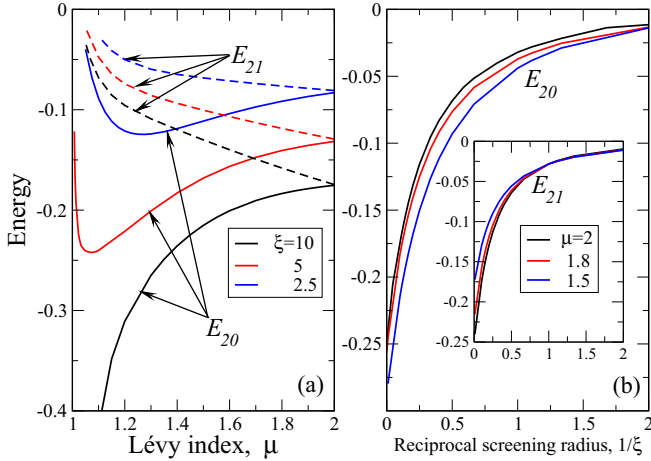
FIG. 2. Same as in Fig. 1 but for the first excited state. In both panels, only the numerical curves are reported. The unscreened case $\xi \to \infty$ is not shown in (a) in order not to clutter the figure. It is qualitatively similar to that for $\xi = 10$. The orbital degeneracy, which takes place at $\mu = 2$ ($E_{21}(\mu = 2) = E_{20}(\mu = 2)$ in (a), is lifted at $\mu < 2$. (b) Portrays the screening radius dependence of E_{20} (main panel) and E_{21} (inset). Values of ξ (a) and μ (b) are coded by colors as shown in the legends.

approach fails. For this reason, in the present problem, we consider the variational method only as an auxiliary one (at $1.5 \lesssim \mu < 2$ and $\xi > 2.5$) for the more accurate numerical treatment.

Because of this, in Fig. 1(b), we report only the numerical dependencies of the ground state energy on the reciprocal (so that the known case of unscreened "ordinary" hydrogen atom corresponds to $1/\xi = 0$) screening radius. This is done for three values of the Lévy index, shown near the corresponding curves. It is seen that in the above "ordinary" case $1/\xi = 0$, $\mu = 2$, the ground state energy equals to -1, which coincides with well-known analytical results $E = -1/n^2$. At lower μ, the curves of ground state energy also decrease monotonically. They run lower than that at $\mu = 2$. This situation is in contrast to the 2D screened case [42], when energy level crossing occurs for the curves with different μ's. As the level crossing may indicate on the quantum chaos (see [43] and references therein) or other extreme disorder manifestations, we speculate that for the 3D case, these effects are absent or highly suppressed. As these chaotic features can disrupt the excitonic device (like solar cell or nanolaser [12,13]) functionality, the latter fact should be taken into account in the designing of devices [based on 2D (heterostructures) and/or 3D (bulk semiconductors)], where exciton properties are essential.

Now we pass to the first excited state. Figure 2 reports the energies of the first excited state, corresponding to the principal quantum number $n = 2$. This case corresponds to $l = 0$ (energy E_{20}) and $l = 1$ (energy E_{21}), see also above, where variational wave functions have been introduced. Similar to the cases of unscreened 3D fractional hydrogenic problems [35] as well as 2D (both screened and unscreened) ones [42,44], the famous orbital degeneracy of a hydrogen atom is lifted at $\mu < 2$. The latter degeneracy is due to the conservation of the Runge-Lenz vector in ordinary 2D and 3D

hydrogenic problems [36,38,39]. Our analysis shows that in the fractional problem, Runge-Lenz vector nonconservation comes from a synergy of disorder and finite screening effects. It should be noted that the degeneracy concerning magnetic quantum number $m \leftrightarrow -m$ is due to the time-inversion symmetry [39] of our problem. It remains in our fractional case. To lift it, an external magnetic field is needed. Our preliminary analysis shows that in this case many interesting effects can be realized. In this case, the magnetic field plays a role of additional (to the disorder, which we consider phenomenologically by the introduction of the fractional Laplacian in our hydrogenic model) external stimulus, which permits to control the properties of our "disordered exciton." For instance, at some magnetic field values, the energy levels crossing and even overlay may occur in a system. This is a direct manifestation of quantum chaotic behavior [43], which may destroy the exciton and cause the problems in device functionality. To check this, it is necessary to consider the classical counterpart of our quantum problem, where possible chaotic trajectories will be immediately revealed [45]. We postpone the studies of these interesting effects to future publications. Figure 2(a) portrays the behavior of E_{20} and E_{21} as functions of Lévy index μ at three fixed values of screening radius ξ. We did not show the unscreened case $\xi \to \infty$ as it is qualitatively similar to that for $\xi = 10$ (weak screening) but will clutter the panel. We note that at $\mu = 2$ (ordinary, i.e., "nonfractional" case) the energies $E_{20} = E_{21}$ signifying the above orbital degeneracy. It is seen that both at strong (small ξ) and weak (large ξ) screenings E_{21} grows going to plus infinity at $\mu \to 1$. At the same time, the energy E_{20} behaves differently at strong ($\xi \leqslant 5$) and weak ($\xi \geqslant 10$) screenings. Namely, in the latter case of weak screening, E_{20} is a monotonous function of μ, going to minus infinity at $\mu \to 1$. On the other hand, at $\xi \leqslant 5$ this function has a minimum, going to plus infinity at $\mu \to 1$. It is seen that at smaller ξ, the minimum becomes shallower and shifts toward $\mu = 2$ so that at $\xi \to 0$ (complete screening) the energy E_{20} starts to behave similarly to E_{21}. The latter effect is absent in "ordinary" (i.e., without fractional derivatives) screened hydrogenic problems, which signifies that in highly disordered semiconductors, the screening effects play a very important role in the excitons' properties. It is also very important for the devices, using transitions between levels with different l's.

The qualitative features of E_{20} and E_{21} behavior as functions of screening radius ξ are already seen from Fig. 2(a). However, the more detailed ξ dependencies are shown in Fig. 2(b). First, it is seen that for the unscreened case $1/\xi = 0$ both curves E_{20} and E_{21}, corresponding to $\mu = 2$ (ordinary, i.e., "nonfractional" case), go to -0.25, which is dictated by "unscreened expression" $E = -1/n^2$ for $n = 2$. Another important feature, which is revealed in Fig. 2(b), is the comparison of ξ dependencies of E_{20} (main panel) and E_{21} (inset) at different Lévy indices μ. Namely, if E_{20} at lower μ goes below that at higher μ in the entire domain of $1/\xi$ values, for E_{21} the situation is different. As curves $E_{21}(\xi)$ at $1.5 < \mu < 2$ are almost indistinguishable at $1 < 1/\xi < 2$ [inset in Fig. 2(b)], our more detailed calculations show that in this range of $1/\xi$, the regularity for E_{21} is similar to that for E_{20}, i.e., $E_{21}(\mu = 1.5) < E_{21}(\mu = 1.8) < E_{21}(\mu = 2)$. At the same time, it is seen that at $1/\xi < 1$ the situation is opposite, i.e., the lowest

curve is $E_{21}(\mu = 2)$, while the highest one is that for $\mu = 1.5$. Our calculations also reveal that the level crossing occurs at $\xi \approx 1$. This means that the joint action of screening and disorder (mimicked here by fractional Laplacian) may cause chaotic behavior for the excited states of "fractional excitons." The detailed studies of this question, both for first and higher excited states, will be published elsewhere.

If considered higher excited states, their main difference from the first one is that there are much (for high n and l) more states, which are no more degenerate at $\mu < 2$. Really, if for $n = 2$ (first excited state), we have four states with radial parts defined by Eqs. (17) and (18), for $n = 3$ (second excited state) we have already nine states with three distinct radial functions. For arbitrary n we have n^2 states with n different radial functions, which makes their detailed studies progressively more cumbersome and time consuming.

Our calculations of the exciton wave functions (not shown) reveals that they are qualitatively similar to those for the unscreened case [35]. The only difference is that while for strong screening (small ξ or large $1/\xi$) as μ goes from two to one, the wave functions become gradually less localized in momentum space, for weak screening the situation is opposite. Specifically, for strong screening, the wave functions amplitudes diminish as $\mu \to 1$ so that they become almost delocalized with zero amplitude. This situation corresponds to extra strong localization in coordinate space, where ψ degenerates into (almost) Dirac δ function, reflecting the exciton collapse. At the same time, for weak screening in momentum space, the wave function resembles Dirac δ function shape as $\mu \to 1$. In coordinate space this generates an almost delocalized wave function, corresponding to exciton ionization. This shows that the interplay between screening and strong disorder (like substance amorphization) may cause excitons to be destroyed (either ionized or collapsed, depending on the relation between screening radius ξ, Lévy index μ, and quantum number l, see above) the excitons, which may prevent the operation of the devices such as solar cells and/or light emitting diodes.

V. DISCUSSION AND CONCLUSIONS

In the spirit of the above picture of exciton wave function localization in coordinate and momentum spaces, it is reasonable to calculate the exciton localization radius, which is an important physical characteristic, which can be readily observed in the experiments. The exciton localization radius is the mean value of radiusvector r in its ground state

$$\bar{r} = \int r \Psi_{10}^2(\mathbf{r}) d^3 r, \tag{22}$$

where $\Psi_{10}(\mathbf{r})$ is the ground state wave function in coordinate space, i.e., the Fourier image of that in momentum space. Figure 3 reports the results of numerical calculation of $\bar{r}$. While at $\xi > 2.5$ the exciton localization radius decays monotonically as μ (imitating the degree of disorder in our problem) approaches one, it is seen that at $\xi = 2.5$ it starts to grow indicating the exciton ionization (i.e., falling apart) at $\mu = 1$. This is a reflection of the fact that the exciton (i.e., bound state of an electron and hole) is destroyed by the synergy of strong screening and disorder, which causes its ionization at $\mu = 1$.
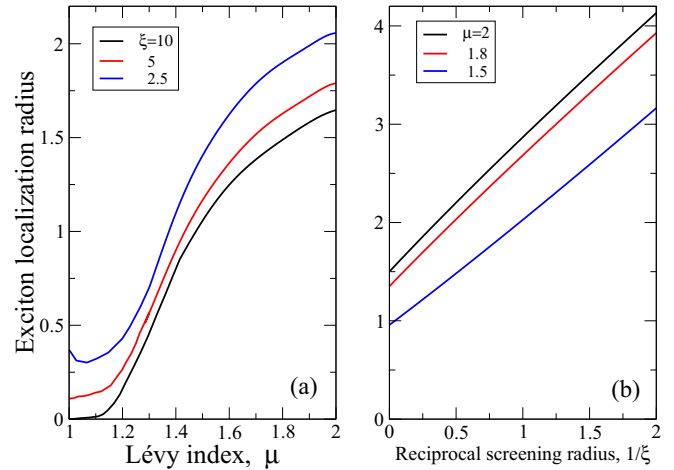

FIG. 3. Exciton localization radius $\bar{r}$, calculated numerically. (a) Reports the dependence on Lévy index μ for three fixed ξ's, coded by colors (legend). (b) Portrays the dependence on $1/\xi$ at fixed μ, also coded by colors and shown in the legend.

This effect has already been shown in Fig. 3, where ground state energy at $\xi = 2.5$ and $\mu = 1$ was zero. Note that at weak screening, the disorder enhances the bound state, which may be viewed as a type of Anderson localization [46], leading to exciton collapse (zero localization radius) at $\mu = 1$.

Panel (b) of Fig. 3 portrays the dependence $\bar{r}(\xi)$ at three fixed values of Lévy index μ: $\mu = 2$ (ordered case), $\mu = 1.8$ (weakly disordered case), and $\mu = 1.5$ (disordered case). It is seen that the exciton localization radius grows with ξ in accord with Figs. 1 and 2, where it has been demonstrated that screening breaks the bound state between electron and hole in an exciton. Also, in the disordered case, the exciton localization radius is smaller than that for $\mu = 2$ for the same ξ. This shows that disorder, characterized by the Lévy index, stabilizes the exciton, preventing its ionization. Thus, to some extent, the disorder and screening are playing opposite roles in the exciton formation: the disorder tends to make it "more localized" (similar to Anderson localization [46]), while screening directs toward the exciton ionization. On the other hand, a very strong disorder, occurring in our system at $\mu \to 1$ makes the exciton collapse. This balance is very important and should be taken into account in the design of corresponding electronic devices. Our estimations show that for moderate (i.e., exciton is not prone to collapse) strength of disorder $\mu = 1.5$, the screening radius r_0, corresponding to dimensionless $\xi = 5.0$ is 50 Å, which is in qualitative agreement with known value for CdS $r_0 = 58$ Å[47,48].

Discussed physical properties of a "screened exciton" related to the interplay between screening and disorder can alter the exciton-exciton interaction in a substance. Namely, the exciton radii ($\bar{r} \sim 5$ nm, which is of the order of 10 lattice constants) presented in Fig. 3 are characterized by dipole moments $e\bar{r}$ (e is the electronic charge), giving rise to multiexciton configurations. On the other hand, these fields will be screened so that many disorder constituents (like defects and impurities) will fall in the span of the above exciton radius. As we have mentioned above, in the semiconductors with different degrees of disorder (different μ's) such a

random screened exciton-exciton interaction may lead either to exciton ionization (high screenings) or to the collapse (low screening) at $\mu = 1$. The described effects can also play an important role in the energy relaxation of electrons and holes, bound in an exciton. In a disordered substance, instead of a process with well-defined time dependence, the energy relaxation from a highly excited to the ground state may become chaotic. Both these processes will have a detrimental effect on the optoelectronic and/or spintronic device functionalities since the disorder may reduce its controllability.

Note that just as the ordinary hydrogenic model of an exciton is limited by the real band structure of a semiconductor sample, our fractional model is also limited by a strong disorder found in (amorphous) substances without translational symmetry. This results in the above distinctly different behavior at extremely strong disorder, corresponding in our model to the case $\mu \to 1$. Namely, while for ground state the exciton collapses, i.e., its ground state energy $E_{g.s.} \to -\infty$ at $\mu \to 1$, for the excited states (depending on orbital quantum number l) it rather ionizes, i.e., decays. To elucidate this feature further, we need to consider weak disorder in our model, corresponding to $\mu \to 2$. In this case, the destruction of the energy bands in a sample can be considered perturbatively. Such calculations would permit to fathom at which degree of disorder (i.e., Lévy index μ) the translational symmetry of the initial (undoped) sample becomes irrelevant. The effects of transition from weak (where band effects can be approximately taken into account) to strong disorder in our approach are currently studied and will be published elsewhere.

Perhaps the main message of the present paper is that the synergy between the screening of Coulomb interaction and disorder in dielectrics (actually semiconductors) generates a corps of properties, which do not occur in ordered substances. Our main supposition here is that Laskin's construction of path integrals with Lévy measure [31] is equivalent to extraction of probability density function from fractional Langevin equation and, in turn, to the assumptions made in the seminal Anderson paper [46]. This (along with the fact that as the width of initial distribution grows, the exciton wave function becomes progressively more localized) permits us to assert that fractional Schrödinger equation accounts for disorder phenomenologically with Lévy index μ being the indicator of its degree. The fact that "free" (i.e., in the systems without external potential) Lévy distributions do not have higher moments [22–26,28] demonstrates that such a construction describes the systems with broad (wider than Gaussian) distribution of their Brownian paths in a generalized Lévy sense. It is almost sure that the physical origin of such broad distribution in solids is disorder. The presence of potential (screened

Coulomb interaction in our case) in the system tames the initial Lévy distribution, making it decay faster than that in a corresponding free problem. In other words, here once more we have an interplay between the breadth of disorder distribution [46] and system potential, which makes the probability distribution (square of the related wave function's modulus) decay faster in space. This makes our problem of a fractional Schrödinger equation resemble an Anderson localization in disordered systems.

As we have shown above, our fractional hydrogenic problem is important for the description of Rydberg excitons in disordered semiconductors. The disorder, influencing the charge carrier (electron or hole in semiconductors) diffusion lengths, may generate the spectrum of excitons, which cannot be described by the Schrödinger equation with ordinary Laplacian. In this case, fractional derivatives should be introduced to describe the situation adequately. The typical example here is semiconducting perovskites like $CsPbBr_3$, which have very long diffusion lengths [49]. The influence of disorder on their excitonic properties plays an important role in their photovoltaic, optoelectronic, and spintronic (especially with Rashba spin-orbit coupling (SOC) [50]) applications. The primary reason is that the above semiconductors have strong SOC, which alters their excitonic spectra, especially in a disordered case [49,51,52]. This is closely related to the chaotic features in the spectra of excitons due to Rashba SOC [43,45]. This suggests one more generalization of our hydrogenic problem. Namely, the spin-orbit interaction term can be added to the corresponding fractional Schrödinger equation. In this case, the solution will be more sophisticated as the wave function will be spinor now [43,53], although the problem can become doable in the momentum space similar to our present case. This problem turns out to be vastly important for many kinds of semiconductors (including $CsPbBr_3$) [49,51,54], where SOC has a profound influence on the optoelectronic, spintronic, and/or photovoltaic devices functionality.

[1] M. Saliba, S. Orlandi, T. Matsui, S. Aghazada, M. Cavazzini, J.-P. Correa-Baena, P. Gao, R. Scopelliti, E. Mosconi, K.-H. Dahmen *et al.*, A molecularly engineered hole-transporting material for efficient perovskite solar cells, Nat. Energy **1**, 15017 (2016).

[2] A. Köhler and H. Bässler, *Electronic Processes in Organic Semiconductors: An Introduction* (John Wiley and Sons, Weinheim, Germany, 2015).

[3] M. Aßmann, J. Thewes, D. Fröhlich, and M. Bayer, Quantum chaos and breaking of all anti-unitary symmetries in Rydberg excitons, Nat. Mater. **15**, 741 (2016).

[4] J. Heckötter, M. Freitag, D. Fröhlich, M. Aßmann, M. Bayer, M. A. Semina, and M. M. Glazov, Scaling laws of Rydberg excitons, Phys. Rev. B **96**, 125142 (2017).

[5] M. Ansari-Rad and S. Athanasopoulos, Theoretical study of equilibrium and nonequilibrium exciton dynamics

in disordered semiconductors, Phys. Rev. B **98**, 085204 (2018).

[6] G. M. Akselrod, F. Prins, L. V. Poulikakos, E. M. Lee, M. C. Weidman, A. J. Mork, A. P. Willard, V. Bulović, and W. A. Tisdale, Subdiffusive exciton transport in quantum dot solids, Nano Lett. **14**, 3556 (2014).

[7] S. M. Ryabchenko, Yu. G. Semenov, and O. V. Terletskii, Broadening of exciton bands in semimagnetic semiconductor $Cd_{1-x}Mn_xTe$ caused by compositional fluctuations, Fizika Tverdogo Tela **27**, 2901 (1985).

[8] C. J. Bardeen, The Structure and dynamics of molecular excitons, Annu. Rev. Phys. Chem. **65**, 127 (2014).

[9] D. Geißler and N. Hildebrandt, Recent developments in Förster resonance energy transfer (FRET) diagnostics using quantum dots, Anal. Bioanal. Chem. **408**, 4475 (2016).

[10] M. Pope and C. E. Swenberg, *Electronic Processes in Organic Crystals and Polymers* (Oxford University Press, New York, 1999).

[11] B. I. Shklovskii and A. L. Efros, *Electronic Properties of Doped Semiconductors* (Springer, Berlin, 1984).

[12] G. Xing, N. Mathews, S. S. Lim, N. Yantara, X. Liu, D. Sabba, M. Grätzel, S. Mhaisalkar, and T. C. Sum, Low-temperature solution-processed wavelength–tunable perovskites for lasing, Nat. Mater. **13**, 476 (2014).

[13] H. Zhu, Y. Fu, F. Meng, X. Wu, Z. Gong, Q. Ding, M. V. Gustafsson, M. T. Trinh, S. Jin, and X. Y. Zhu, Lead halide perovskite nanowire lasers with low lasing thresholds and high quality factors, Nat. Mater. **14**, 636 (2015).

[14] B. D. Hughes, *Random Walks and Random Environments* (Clarendon Press, Oxford, 1995), Vol. 1.

[15] C. Cohen-Tannoudji and D. Guéry-Odelin, *Advances in Atomic Physics. An overview* (World Scientific, Singapore, 2011).

[16] S. Marksteiner, K. Ellinger, and P. Zoller, Anomalous diffusion and Lévy walks in optical lattices, Phys. Rev. A **53**, 3409 (1996).

[17] S. A. Gredeskul and Yu. S. Kivshar, Propagation and scattering of nonlinear waves in disordered systems, Phys. Rep. **216**, 1 (1992).

[18] H. Katori, S. Schlipf, and H. Walther, Anomalous Dynamics of a Single Ion in an Optical Lattice, Phys. Rev. Lett. **79**, 2221 (1997).

[19] H. Scher and E. M. Montroll, Anomalous transit-time dispersion in amorphous solids, Phys. Rev. B **12**, 2455 (1975).

[20] G. Pfister and H. Scher, Dispersive (non-Gaussian) transient transport in disordered solids, Adv. Phys. **27**, 747 (1978).

[21] E. Lucioni, B. Deissler, L. Tanzi, G. Roati, M. Zaccanti, M. Modugno, M. Larcher, F. Dalfovo, M. Inguscio, and G. Modugno, Observation of Subdiffusion in a Disordered Interacting System, Phys. Rev. Lett. **106**, 230403 (2011).

[22] S. G. Samko, A. A. Kilbas, and O. I. Maritchev, *Fractional Integrals and Derivatives* (Gordon and Breach, New York, 2003).

[23] I. Podlubny, *Fractional Differential Equations* (Academic Press, 1999).

[24] P. Lévy, *Théorie de l'Addition des Variables Aléatoires* (Gauthier-Villars, Paris, 1954).

[25] G. Samorodnitsky and M. S. Taqqu, *Stable Non-Gaussian Random Processes* (Chapman and Hall, New York, 1994).

[26] R. Metzler and J. Klafter, The restaurant at the end of the random walk: Recent developments in the description of

anomalous transport by fractional dynamics, J. Phys. A: Math. Gen. **37**, R161 (2004).

[27] G. M. Zaslavsky, *Hamiltonian Chaos and Fractional Dynamics* (Oxford University Press, New York, 2005).

[28] R. Metzler, J.-H. Jeon, A. G. Cherstvy, and E. Barkai, Anomalous diffusion models and their properties: Non-stationarity, non-ergodicity, and ageing at the centenary of single particle tracking, Phys. Chem. Chem. Phys. **16**, 24128 (2014).

[29] R. N. Mantegna and H. E. Stanley, *An Introduction to Econophysics. Correlations and Complexity in Finance* (Cambridge University Press, Cambridge, 2000).

[30] S. Rachev, Y. Kim, M. Bianchi, and F. Fabozzi, *Financial Models with Lévy Processes and Volatility Clustering* (Wiley, New York, 2011).

[31] N. Laskin, *Fractional Quantum Mechanics* (World Scientific, Singapore, 2018).

[32] *Handbook of Mathematical Functions*, edited by M. Abramowitz and I. Stegun (Dover, New York, 1972).

[33] A. I. Anselm, *Introduction to Semiconductor Theory* (Englewood Cliffs, N. J., Prenctice-Hall, 1981).

[34] N. W. Ashkroft and N. D. Mermin, *Solid State Physics* (Harcourt, New York, 1976).

[35] V. A. Stephanovich and W. Olchawa, Lévy distributions and disorder in excitonic spectra, Phys. Chem. Chem. Phys. **22**, 24462 (2020).

[36] S. Flügge, *Practical Quantum Mechanics* (Springer, Berlin, 1999).

[37] V. A. Fock, Zur Theorie des Wasserstoffatoms, Z. Phys. **98**, 145 (1935).

[38] M. Lévy, Wave equations in momentum space, Proc. Royal Soc. of London. Series A **204**, 145 (1950).

[39] L. D. Landau and E. M. Lifshits, *Quantum Mechanics. Nonrelativistic Theory* (Pergamon Press, Oxford, 1995).

[40] B. Podolsky and L. Pauling, The momentum distribution in hydrogen–like atoms, Phys. Rev. **34**, 109 (1929).

[41] A. D. Polyanin and A. V. Manzhirov, *Handbook of Integral Equations* (Chapman and Hall/CRC Press, Boca Raton-London, 2008).

[42] E. V. Kirichenko and V. A. Stephanovich, The influence of Coulomb interaction screening on the excitons in disordered two'dimensional insulators, Sci. Rep. **11**, 11956 (2021).

[43] V. A. Stephanovich, E. Ya. Sherman, N. T. Zinner, and O. V. Marchukov Energy-level repulsion by spin-orbit coupling in two-dimensional Rydberg excitons, Phys. Rev. B **97**, 205407 (2018).

[44] E. V. Kirichenko and V. A. Stephanovich, The influence of disorder on the exciton spectra in two-dimensional structures, Phys. Chem. Chem. Phys. **21**, 21847 (2019).

[45] V. A. Stephanovich and E. Ya. Sherman, Chaotization of internal motion of excitons in ultrathin layers by spin-orbit coupling, Phys. Chem. Chem. Phys. **20**, 7836 (2018).

[46] P. W. Anderson, Absence of diffusion in certain random lattices, Phys. Rev. **109**, 1492 (1958).

[47] A. Franceschetti, H. Fu, L. W. Wang, and A. Zunger, Many-body pseudopotential theory of excitons in InP and CdSe quantum dots, Phys. Rev. B **60**, 1819 (1999).

[48] N. Razgoniaeva, P. Moroz, M. Yang, D. S. Budkina, H. Eckard, M. Augspurger, D. Khon, A. N. Tarnovsky, and M. Zamkov, One-dimensional carrier confinement in giant CdS/CdSe excitonic nanoshells, J. Am. Chem. Soc. **139**, 7815 (2017).

[49] S. D. Stranks and H. J. Snaith, Metal-halide perovskites for photovoltaic and light-emitting devices, Nat. Nanotechnol. **10**, 391 (2015).

[50] Yu. A. Bychkov and E. I. Rashba, Properties of a 2D electron gas with lifted spectral degeneracy, JETP Lett. **39**, 78 (1984).

[51] D. Canneson, E. V. Shornikova, D. R. Yakovlev, T. Rogge, A. A. Mitioglu, M. V. Ballottin, P. C. M. Christianen, E. Lhuillier, M. Bayer, and L. Biadala, Negatively charged and dark excitons in CsPbBr$_3$ perovskite nanocrystals revealed by high magnetic fields, Nano Lett. **17**, 6177 (2017).

[52] M. Fu, Ph. Tamarat, H. Huang, J. Even, A. L. Rogach, and B. Lounis, Neutral and charged exciton fine structure in single lead halide perovskite nanocrystals revealed by magneto-optical spectroscopy, Nano Lett. **17**, 2895 (2017).

[53] C. Grimaldi, Energy levels of a two-dimensional hydrogen atom with spin-orbit Rashba interaction, Phys. Rev. B **77**, 113308 (2008).

[54] W. S. Yang, J. H. Noh, N. J. Jeon, Y. C. Kim, S. Ryu, J. Seo, and S. I. Seok, Solar cells. High-performance photovoltaic perovskite layers fabricated through intramolecular exchange, Science **348**, 1234 (2015).